Letters

Couplings in Phase Domain Impedance Modeling of Grid-Connected Converters

Mohammad Kazem Bakhshizadeh, *Student Member, IEEE*, Xiongfei Wang, *Member, IEEE*, Frede Blaabjerg, *Fellow, IEEE*, Jesper Hjerrild, Łukasz Kocewiak, *Member, IEEE*, Claus Leth Bak, *Senior Member, IEEE*, and Bo Hesselbæk

***Abstract*—The output impedance of a power converter plays an important role in the stability assessment of the converter. The impedance can be expressed in different frames such as the stationary frame (phase domain) or in the synchronous frame (*dq* domain). To treat the three-phase system like a single-phase system, the system can be divided into positive and negative sequences in the phase domain. This paper demonstrates that there exist couplings between the positive and negative sequences, even in a balanced system due to the PLL, which is important for synchronization. Further it will be shown that even though these couplings are very small in magnitude, they are important in the stability of the converter.**

***Index Terms*—Grid-connected inverters, harmonic stability, impedance modeling.**

I. Introduction

More and more power electronic components are being used in electric power systems, including renewable energy sources [1], high-voltage dc transmission system [2], and also microgrids [3]. Despite the advantages of power electronic converters such as high efficiency and controllability, they may inject high order harmonics that if they are left uncontrolled may trigger the parallel and series resonances in the power system [4]. The interaction between the passive components such as line/cable impedances, filters and active components may further result in instability [5], [6].

In [7], it has been shown that a converter, including the control systems and passive filters can be modeled as an output impedance connected to a voltage/current source. Therefore, the interaction between converters, passive components, and the grid can be evaluated by the impedance-based stability criterion [8]–[10].

In [11], the impedance of a balanced three-phase converter by considering a PLL has been developed, which simply assumes that the impedances are decoupled in positive and negative sequences. The impedance could also be represented in the *dq*-domain as a matrix [12]–[16]. In [14], the stability of ac systems has been analyzed using the measured *dq* frame impedances. Due to the cross couplings in the impedance matrix in the *dq* frame, the normal Nyquist criterion cannot be used, and the Generalized Nyquist Criterion (GNC) should be utilized instead [16].

This paper shows that the impedance in the phase domain also has cross couplings between the positive and negative sequences, which are found to be important in the stability assessment of a power converter. Experimental results validate this finding too.

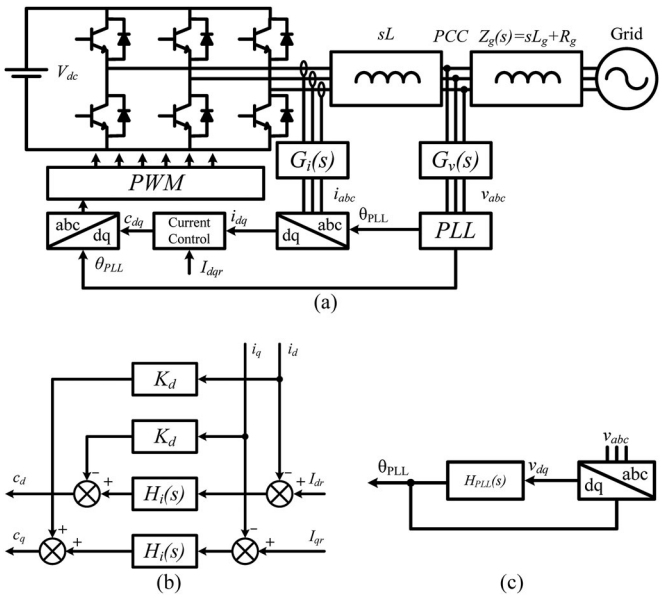

Fig. 1. Current controlled three-phase converter. (a) Circuit topology to the grid. (b) Current controllers. (c) PLL block.

II. Problems in Neglecting the Couplings Between Sequences

The three-phase converter considered in this paper is shown in Fig. 1(a). In order to make the problem simpler, the dc bus is considered to be stiff and constant. It is assumed that the system is balanced and the converter is injecting active and reactive currents ($I_{\rm dr}$ and $I_{\rm qr}$) into the grid.

Fig. 1(b) shows the *dq*-domain current controller, where $H_i(s)$ is a PI regulator to control the *dq* components of the output current, and K_d is the decoupling term to improve the control dynamics. Fig. 1(c) depicts a basic PLL known as

Manuscript received January 22, 2016; revised February 22, 2016; accepted March 3, 2016. Date of publication March 28, 2016; date of current version May 20, 2016. This work was supported in part by the DONG Energy Wind Power A/S and in part by the Innovation Fund Denmark.

M. K. Bakhshizadeh, J. Hjerrild, Ł. Kocewiak, and B. Hesselbæk are with the DONG Energy Wind Power, Fredericia 7000, Denmark (e-mail: mok@et.aau.dk; jeshj@dongenergy.dk; lukko@dongenergy.dk; bohes@dongenergy.dk).

X. Wang, F. Blaabjerg, and C. L. Bak are with the Department of Energy Technology, Aalborg University, Aalborg DK-9220, Denmark (e-mail: xwa@et.aau.dk; fbl@et.aau.dk; clb@et.aau.dk).

Color versions of one or more of the figures in this paper are available online at http://ieeexplore.ieee.org.

Digital Object Identifier 10.1109/TPEL.2016.2542244

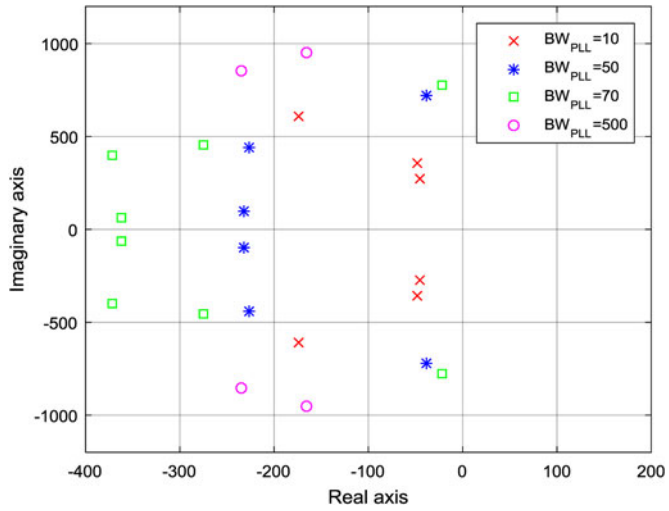

Fig. 2. Closed loop poles of the grid-connected inverter using [11] for different bandwidths of the PLL.

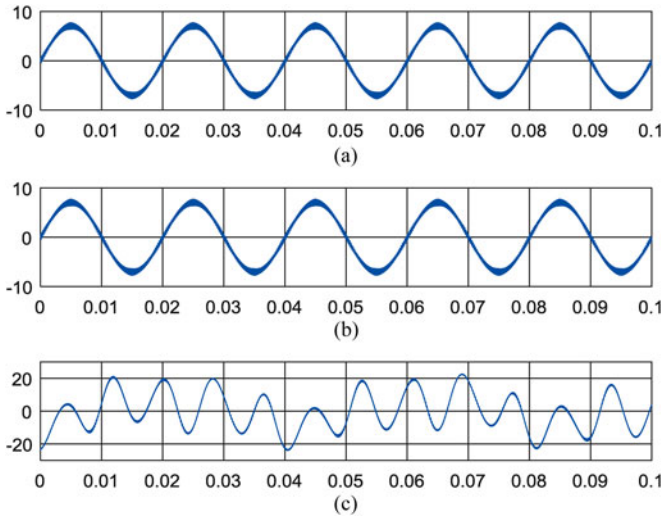

Fig. 3. Simulation results of the injected current of the system in Fig. 1 for (a) $BW_{\mathrm{PLL}} = 10\,\mathrm{Hz}$ (b) $BW_{\mathrm{PLL}} = 50\,\mathrm{Hz}$ (c) $BW_{\mathrm{PLL}} = 70\,\mathrm{Hz}$.

TABLE I
PARAMETERS OF GRID-CONNECTED INVERTER FOR SIMULATION

Symbol	Description	Value
V_g	Grid line-ground peak voltage	90 V
f_1	Grid frequency	50 Hz
L_g	Grid inductance	3 mH
R_g	Grid equivalent resistance	0.5 Ω
V_{dc}	Inverter dc voltage	300 V
I_{dr}	d channel current reference	7 A
I_{qr}	q channel current reference	0 A
K_p	Proportional gain of the current controller	0.01
K_i	Integrator gain of current controller	3
BW_{PLL}	Bandwidth of PLL (Stable)	50 Hz
	(Unstable)	70 Hz
K_d	Decoupling term	0
f_s	Sampling frequency	5 kHz
f_{sw}	Switching frequency	5 kHz
G_v	Transfer function of the sampling circuit for voltage	$\frac{1}{0.00044\,s+1}$
G_i	Transfer function of the sampling circuit for current	$\frac{1}{0.00044\,s+1}$

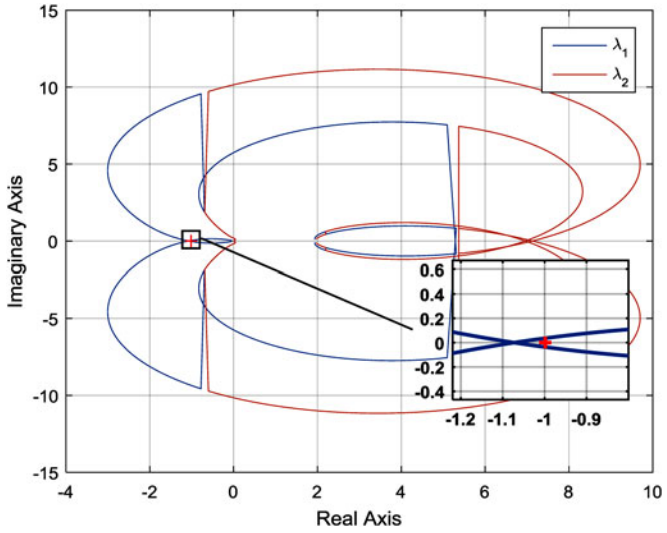

Fig. 4. Generalized Nyquist plot in *dq* domain using the approach proposed in [12] ($\mathrm{BW}_{\mathrm{PLL}} = 70\,\mathrm{Hz}$).

the Synchronous Reference Frame PLL (SRF-PLL), where $H_{\mathrm{PLL}}(s)$ is the loop compensator.

In [11], the positive- and negative-sequence impedances of a power converter have been obtained and it has been shown the positive sequence voltage has no effect on the negative sequence current. If the grid impedance is also decoupled, then the stability can be assessed by examining the poles of

$$\begin{cases} V_{\mathrm{PCC-p}} = v_p Z_{P-\mathrm{conv}} / \left(Z_{P-\mathrm{conv}} + Z_{P-\mathrm{grid}}\right) \\ V_{\mathrm{PCC-n}} = v_n Z_{N-\mathrm{conv}} / \left(Z_{N-\mathrm{conv}} + Z_{N-\mathrm{grid}}\right) \end{cases} \quad (1)$$

where $Z_{p-\mathrm{conv}}$ and $Z_{n-\mathrm{conv}}$ are the positive- and negative-sequence impedances of the converter. The closed loop poles, which are obtained from (1), are shown in Fig. 2 for a converter, whose parameters are shown in Table I including a specific bandwidth of the PLL (BW_{PLL}). Fig. 2 indicates that for $\mathrm{BW}_{\mathrm{PLL}} = 70\,\mathrm{Hz}$ and even 500 Hz the system should be stable. However, time domain simulation results as shown in Fig. 3 indicate that for $\mathrm{BW}_{\mathrm{PLL}} = 70\,\mathrm{Hz}$, the system, even a balanced system, is unstable.

The impedance of the converter in the *dq* domain is a 2×2 matrix with nonzero off-diagonal elements [12]. Therefore, the GNC method must be used for

$$L = [Z_{dq-\mathrm{grid}}] \times [Z_{dq-\mathrm{conv}}]^{-1}. \quad (2)$$

Fig. 4 shows the GNC plot, where $\mathrm{BW}_{\mathrm{PLL}}$ is 70 Hz and validates the simulation results that for PLL bandwidth beyond 70 Hz the system is unstable.

III. COUPLINGS BETWEEN NEGATIVE AND POSITIVE SEQUENCE

One way to find the frequency-dependent impedance of the converter is to perturb the input voltage with a certain frequency

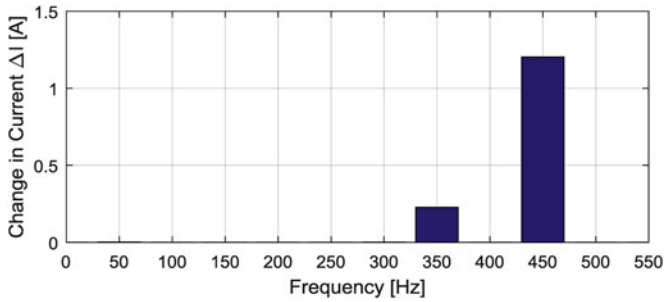

Fig. 5. Frequency spectrum of the output current when a positive sequence perturbation at 450 Hz is applied.

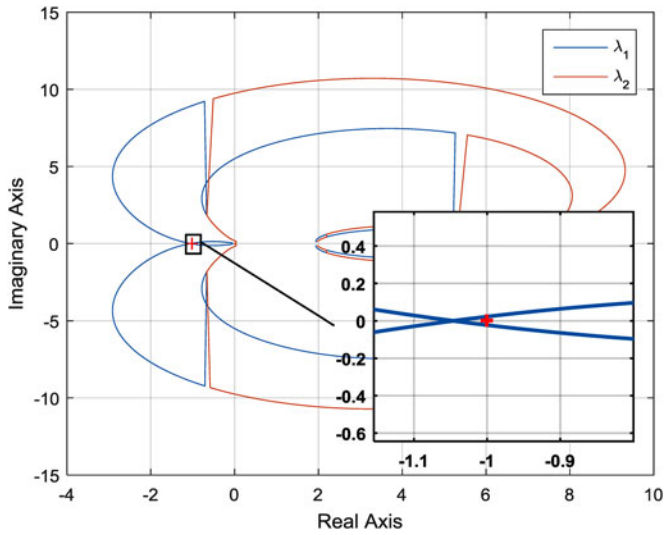

Fig. 6. Generalized Nyquist plot using (4) in phase domain ($\mathrm{BW_{PLL}} = 70$ Hz).

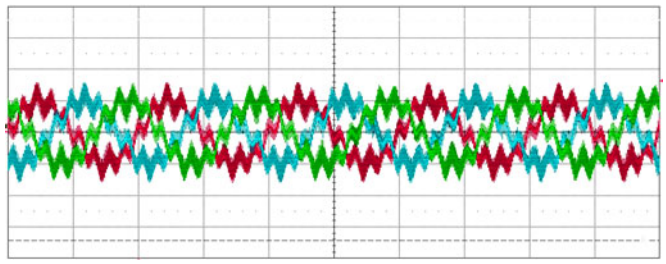

Fig. 7. Experimental results of the output current when a positive sequence perturbation at 450 Hz is applied (5 A/div and 10 ms/div).

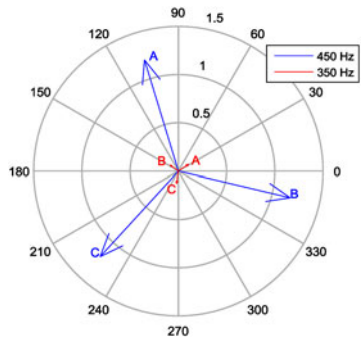

Fig. 8. Phasor diagram of the current response to a 450 Hz perturbation.

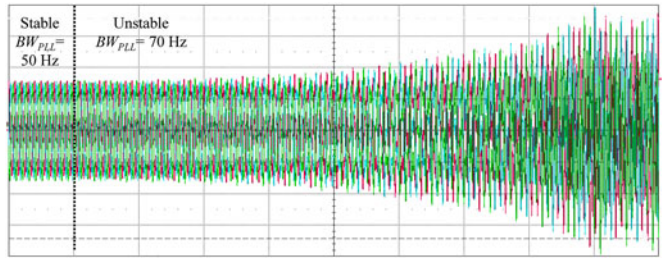

Fig. 9. Instability due to the change of the PLL bandwidth ($\mathrm{BW_{PLL}}$) from 50 Hz to 70 Hz (5A/div and 10 ms/div).

and study the current response of the converter in a steady state. The change in amplitude and phase shift specifies the impedance at that frequency [11].

Fig. 5 shows the converter response to a 450-Hz positive-sequence voltage perturbation, which is a small signal and it is injected in series with the grid. It can be seen that in addition to the 450 Hz component, there is also a 350 Hz component, which is negative sequence. The response of a linear and positive sequence impedance in a steady state contains only one component with the same frequency and sequence of the perturbation. Therefore, this additional component indicates that there must be a frequency and sequence couplings. The full admittance matrix, which is derived in Appendix, is as follows:

$$Y_{\mathrm{PN}} = \begin{bmatrix} Y_p(s) & J_n(s-2j\omega_1) \\ J_p(s) & Y_n(s-2j\omega_1) \end{bmatrix}. \tag{3}$$

It can be seen in (3) that the impedance matrix has cross couplings. Similarly to (2) [12], and according to the impedance-based stability criterion [8], the GNC must be used for (4) to assess the stability. The frequency shifts in (3) and (4) are used for modeling the frequency couplings

$$L = \begin{bmatrix} Z_{g-p}(s) & 0 \\ 0 & Z_{g-n}(s-2j\omega_1) \end{bmatrix} \times Y_{\mathrm{PN}}. \tag{4}$$

Fig. 6 shows the GNC plot derived from (4), which is almost the same as Fig. 4, in which impedance modeling in *dq* domain is used. This also implies that the coupling must be considered no matter in which frame the impedance model of the converter is derived, and all the models should have the same stability implications.

IV. Experimental Results

In order to verify the discussed couplings and their effects on the converter stability, a low power prototype with the parameters listed in Table I is used.

Fig. 7 shows the current response of the converter to a positive sequence perturbation at 450 Hz. This perturbation is applied

using a Chroma 61845 regenerative grid simulator. Fig. 8 shows the phasor diagrams of the harmonics of the current response. It is evident that in addition to the perturbation frequency, there is also another component at 350 Hz ($f_p - 2f_1$), which has a negative sequence.

Fig. 9 verifies the theory and the simulation results, which shows that when the bandwidth of the PLL is changed from 50 to 70 Hz, the system becomes unstable.

V. Conclusion

In this paper, it has been shown that the impedance of a three-phase converter, which is operating in balanced conditions, cannot be modeled as pure positive- or negative-sequence impedances. Instead very similar to modeling the impedance in the *dq* domain, modeling in phase domain also leads to an impedance matrix, which relates the positive and negative sequences together. Neglecting the small coupling term results in a wrong estimation of power converter's stability.

Appendix

Since this paper models the impedance in the phase domain, both positive- and negative-sequence perturbations are investigated. In time domain the Phase A voltage is represented as [11]

$$\begin{aligned} v_a(t) = {} & V_1 \cos(\omega_1 t) + V_p \cos(\omega_p t + \phi_p) \\ & + V_n \cos(\omega_n t + \phi_n)\, V_p, V_n \ll V_1 \end{aligned} \tag{A.1}$$

where ω_1 is the system base frequency, V_1 is the fundamental voltage at PCC, V_p and V_n are the positive- and negative-sequence perturbations, which are much smaller than V_1. ϕ_p and ϕ_n are the phase shifts of the perturbations. In the frequency domain, the voltage of phase A is given by

$$V_a(f) = \begin{cases} V_1 = V_1/2, & f = \pm f_1 \\ V_p = V_p e^{\pm j\phi_p}/2, & f = \pm f_p \\ V_n = V_n e^{\pm j\phi_n}/2, & f = \pm f_n \end{cases} \tag{A.2}$$

where $\mathbf{V}_\mathrm{p}$ and $\mathbf{V}_\mathrm{n}$ are complex vectors rotating with the specified frequency. Therefore, the current response to the voltage perturbations can be found using the converter average model at two different frequencies

$$LsI_{\mathrm{abc}} = C_{\mathrm{abc}}(s) K_m(s) V_{\mathrm{dc}} - V_{\mathrm{abc}} \tag{A.3}$$

where C_{abc} is the modulating signal, which is the output of the current controller. $K_m(s)$ models the gain and delays (computational and PWM) of the converter, which has a transfer function of

$$K_m(s) = e^{-1.5T_s s} \tag{A.4}$$

where T_s is the sampling period.

It must be noted that the detected phase angle of the PLL is affected by the voltage perturbation. Equation (A.5), which can be found in [11], shows the relation between perturbation and the deviation in detected angle as

$$\Delta\theta[f] = \begin{cases} \mp jTF_{\mathrm{PLL}}(s = \pm j(\omega_p - \omega_1))\, \widehat{V}_p, & f = \pm(f_p - f_1) \\ \pm jTF_{\mathrm{PLL}}(s = \pm j(\omega_p - \omega_1))\, \widehat{V}_n, & f = \pm(f_n + f_1) \end{cases}$$

$$TF_{\mathrm{PLL}}(s) = \frac{H_{\mathrm{PLL}}(s)}{1 + H_{\mathrm{PLL}}(s) V_1} \tag{A.5}$$

TABLE II
Frequency Coupling in Response to a Positive/Negative-Sequence Perturbation

Perturbation			Response		
Symbol	Freq.	Seq.	Symbol	Freq.	Seq.
$\mathbf{V}_\mathrm{p}$	f_p	Pos.	$\mathbf{I}_\mathrm{p}$	f_p	Pos.
			$\mathbf{I}_{\mathrm{p}2}$	$f_p - 2f_1$	Neg.
$\mathbf{V}_\mathrm{n}$	f_n	Neg.	$\mathbf{I}_\mathrm{n}$	f_n	Neg.
			$\mathbf{I}_{\mathrm{n}2}$	$f_n + 2f_1$	Pos.

where $G_v(s = \pm j\omega_p)\, V_p$ is replaced by $\widehat{V}_p$ to save space. The Park's and inverse Park's transformations by considering small signal perturbations can be written as follows:

$$T_{\theta_{\mathrm{PLL}}(t)} = \begin{bmatrix} \cos(\Delta\theta) & \sin(\Delta\theta) \\ -\sin(\Delta\theta) & \cos(\Delta\theta) \end{bmatrix} T_{\theta_1(t)} = \begin{bmatrix} 1 & \Delta\theta \\ -\Delta\theta & 1 \end{bmatrix} T_{\theta_1(t)} \tag{A.6}$$

$$T^{-1}_{\theta_{\mathrm{PLL}}} = T^{-1}_{\theta_1} \begin{bmatrix} 1 & -\Delta\theta \\ \Delta\theta & 1 \end{bmatrix}. \tag{A.7}$$

It is evident in Fig. 5 that the output current has two different frequencies. One is the same frequency as perturbed and the same sequence, while the other one has a different frequency and sequence as shown in Table II. If it is assumed that the output current contains the frequencies stated in Table II, then the *dq* components considering the PLL dynamics can be calculated as follows:

$$I_d[f] = \begin{cases} I_{\mathrm{dr}}, & f = dc \\ \widehat{I}_p + \widehat{I}_{p2} + \Delta\theta I_{qr}, & f = \pm(f_p - f_1) \\ \widehat{I}_n + \widehat{I}_{n2} + \Delta\theta I_{qr}, & f = \pm(f_n + f_1) \end{cases} \tag{A.8}$$

$$I_q[f] = \begin{cases} I_{\mathrm{qr}}, & f = dc \\ \mp j\widehat{I}_p \pm j\widehat{I}_{\mathrm{p}2} - \Delta\theta I_{\mathrm{dr}}, & f = \pm(f_p - f_1) \\ \pm j\widehat{I}_n \mp j\widehat{I}_{n2} - \Delta\theta I_{\mathrm{dr}}, & f = \pm(f_n + f_1) \end{cases} \tag{A.9}$$

C_d and C_q, which are the modulating signals in *dq* domain, can be found by

$$\begin{bmatrix} C_d \\ C_q \end{bmatrix} = \begin{bmatrix} -H_i[f] & -K_d \\ K_d & -H_i[f] \end{bmatrix} \begin{bmatrix} I_d \\ I_q \end{bmatrix}. \tag{A.10}$$

Using (A.9) and (A.10) to calculate the modulating signals in the phase domain gives

$$\begin{bmatrix} C_a \\ C_b \\ C_c \end{bmatrix} = T^{-1}_{\theta_1} G_v(\pm j\omega_1) \begin{bmatrix} C_d - C_q\Delta\theta \\ C_d\Delta\theta + C_q \\ 0 \end{bmatrix} = T^{-1}_{\theta_1} \begin{bmatrix} C_{d1} \\ C_{q1} \\ 0 \end{bmatrix} \tag{A.11}$$

$$2C_a = \begin{cases} C_{d1}|_{f=dc} \pm jC_{q1}|_{f=dc}, & f = \pm f_1 \\ C_{d1}\big|_{f=\pm(f_p-f_1)} \pm jC_{q1}\big|_{f=\pm(f_p-f_1)}, & f = \pm f_p \\ C_{d1}\big|_{f=\pm(f_p-f_1)} \mp jC_{q1}\big|_{f=\pm(f_p-f_1)}, & f = \pm(f_p - 2f_1) \cdot \\ C_{d1}\big|_{f=\pm(f_n+f_1)} \mp jC_{q1}\big|_{f=\pm(f_n+f_1)}, & f = \pm f_n \\ C_{d1}\big|_{f=\pm(f_n+f_1)} \pm jC_{q1}\big|_{f=\pm(f_n+f_1)}, & f = \pm(f_n + 2f_1) \end{cases} \tag{A.12}$$

$$Y_p = \frac{1 - V_{\rm dc}K_m(s)G_v(s)TF_{\rm PLL}\left(s-j\omega_1\right)\left(\left(\frac{C_{1d}+jC_{1q}}{2}+\left(\frac{I_{\rm dr}+jI_{\rm qr}}{2}\right)H_i\left(s-j\omega_1\right)\right)\right)}{Ls+V_{\rm dc}K_m(s)G_i\left(s\right)H_i\left(s-j\omega_1\right)} \tag{A.14}$$

$$Y_n = \frac{1 - V_{\rm dc}K_m(s)G_v(s)TF_{\rm PLL}\left(s+j\omega_1\right)\left(\left(\frac{C_{1d}-jC_{1q}}{2}+\left(\frac{I_{\rm dr}-jI_{\rm qr}}{2}\right)H_i\left(s+j\omega_1\right)\right)\right)}{Ls+V_{\rm dc}K_m(s)G_i\left(s\right)H_i\left(s+j\omega_1\right)} \tag{A.15}$$

$$J_p = \frac{V_{\rm dc}K_m\left(s-2j\omega_1\right)G_v(s)G_v\left(-j\omega_1\right)^2TF_{\rm PLL}\left(s-j\omega_1\right)\left(\frac{C_{1d}-jC_{1q}}{2}+\left(\frac{I_{\rm dr}-jI_{\rm qr}}{2}\right)H_i\left(s-j\omega_1\right)\right)}{L\left(s-2j\omega_1\right)+V_{\rm dc}K_m\left(s-2j\omega_1\right)G_i\left(s-2j\omega_1\right)H_i\left(s-j\omega_1\right)} \tag{A.16}$$

$$J_n = \frac{V_{\rm dc}K_m\left(s+2j\omega_1\right)G_v(s)G_v\left(j\omega_1\right)^2TF_{\rm PLL}\left(s+j\omega_1\right)\left(\frac{C_{1d}+jC_{1q}}{2}+\left(\frac{I_{\rm dr}+jI_{\rm qr}}{2}\right)H_i\left(s+j\omega_1\right)\right)}{L\left(s+2j\omega_1\right)+V_{\rm dc}K_m\left(s+2j\omega_1\right)G_i\left(s+2j\omega_1\right)H_i\left(s+j\omega_1\right)} \tag{A.17}$$

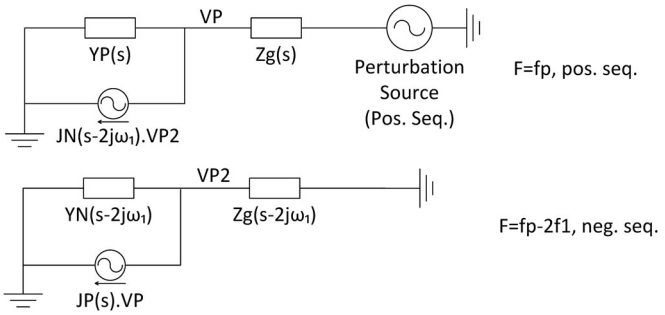

Fig. 10. Equivalent circuit including the grid impedance.

It can be seen from (A.12) that the modulating signal $C_{\rm abc}$ and the consequent converter current $I_{\rm abc}$ only have two frequency components as assumed before (two for each of the positive- and negative-sequence perturbations). Therefore, it verifies that there exist only two frequency components in the current and no more components will appear at any condition. By using (A.3) the current response becomes

$$I_a(f) = \begin{cases} Y_p\widehat{V}_p, & f = f_p, & Pos. \\ J_p\widehat{V}_p, & f = f_p - 2f_1, & Neg. \\ Y_n\widehat{V}_n, & f = f_n, & Neg. \\ J_n\widehat{V}_n, & f = f_n + 2f_1, & Pos. \end{cases} \tag{A.13}$$

where Y_p, Y_n, J_p and J_n are defined in (A.14)–(A.17) shown at the top of the page. Fig. 10 shows the equivalent circuit of the converter in two different sequences and frequencies. It is also worth to note that these coupling terms are present due to the PLL effect. If the PLL is neglected, then the resultant of the coupling terms, (A.16) and (A.17), become zero, because they are directly proportional to $TF_{\rm PLL}$ and $\Delta\theta$.

REFERENCES

[1] F. Blaabjerg, Z. Chen, and S. B. Kjaer, "Power electronics as efficient interface in dispersed power generation systems," *IEEE Trans. Power Electron.*, vol. 19, no. 5, pp. 1184–1194, Sep. 2004.

[2] N. Flourentzou, V. G. Agelidis, and G. D. Demetriades, "VSC-Based HVDC power transmission systems: An overview," *IEEE Trans. Power Electron.*, vol. 24, no. 3, pp. 592–602, Mar. 2009.

[3] J. Rocabert, A. Luna, F. Blaabjerg, and P. Rodriguez, "Control of power converters in AC microgrids," *IEEE Trans. Power Electron.*, vol. 27, no. 11, pp. 4734–4749, Nov. 2012.

[4] Z. Shuai, D. Liu, J. Shen, C. Tu, Y. Cheng, and A. Luo, "Series and parallel resonance problem of wideband frequency harmonic and its elimination strategy," *IEEE Trans. Power Electron.*, vol. 29, no. 4, pp. 1941–1952, Apr. 2014.

[5] P. Brogan, "The stability of multiple, high power, active front end voltage sourced converters when connected to wind farm collector system," in *Proc. Eur. Conf. Power Electron. Appl.*, 2010, pp. 1–6.

[6] J. H. Enslin and P. J. Heskes, "Harmonic interaction between a large number of distributed power inverters and the distribution network," *IEEE Trans. Power Electron.*, vol. 19, no. 6, pp. 1586–1593, Nov. 2004.

[7] R. Middlebrook, "Input filter considerations in design and application of switching regulators," in *Proc. IEEE Ind. Appl. Soc. Annu. Meeting*, 1976, pp. 366–382.

[8] J. Sun, "Impedance-based stability criterion for grid-connected inverters," *IEEE Trans. Power Electron.*, vol. 26, no. 11, pp. 3075–3078, Nov. 2011.

[9] X. Wang, F. Blaabjerg, and W. Wu, "Modeling and analysis of harmonic stability in an AC power-electronics-based power system," *IEEE Trans. Power Electron.*, vol. 29, no. 12, pp. 6421–6432, Dec. 2014.

[10] X. Wang, F. Blaabjerg, M. Liserre, Z. Chen, J. He, and Y. Li, "An active damper for stabilizing power-electronics-based AC systems," *IEEE Trans. Power Electron.*, vol. 29, no. 7, pp. 3318–3329, Jul. 2014.

[11] M. Cespedes and J. Sun, "Impedance modeling and analysis of grid-connected voltage-source converters," *IEEE Trans. Power Electron.*, vol. 29, no. 3, pp. 1254–1261, Mar. 2014.

[12] B. Wen, D. Boroyevich, R. Burgos, P. Mattavelli, and Z. Shen, "Analysis of D-Q small-signal impedance of grid-tied inverters," *IEEE Trans. Power Electron.*, vol. 31, no. 1, pp. 675–687, Jan. 2016.

[13] L. Harnefors, M. Bongiorno, and S. Lundberg, "Input-admittance calculation and shaping for controlled voltage-source converters," *IEEE Trans. Ind. Electron.*, vol. 54, no. 6, pp. 3323 -3334, Dec. 2007.

[14] B. Wen, D. Boroyevich, R. Burgos, P. Mattavelli, and Z. Shen, "Small-signal stability analysis of three-phase AC systems in the presence of constant power loads based on measured d-q frame impedances," *IEEE Trans. Power Electron.*, vol. 30, no. 10, pp. 5952–5963, Oct. 2015.

[15] B. Wen, D. Dong, D. Boroyevich, R. Burgos, P. Mattavelli, and Z. Shen, "Impedance-based analysis of grid-synchronization stability for three-phase paralleled converters," *IEEE Trans. Power Electron.*, vol. 31, no. 1, pp. 26–38, Jan. 2016.

[16] B. Wen, D. Boroyevich, P. Mattavelli, Z. Shen, and R. Burgos, "Experimental verification of the Generalized Nyquist stability criterion for balanced three-phase ac systems in the presence of constant power loads," in *Proc. Energy Convers. Congr. Expo.*, Sep. 2012, pp. 3926–3933.